JACS
JOURNAL OF THE AMERICAN CHEMICAL SOCIETY

ARTICLE

pubs.acs.org/JACS

Dramatic Reduction of IR Vibrational Cross Sections of Molecules Encapsulated in Carbon Nanotubes

Dmitry V. Kazachkin,[†,‡,⊥] Yoshifumi Nishimura,[§,⊥] Henryk A. Witek,[*,∥] Stephan Irle,[*,§] and Eric Borguet[*,†]

[†]Department of Chemistry, Temple University, Philadelphia, Pennsylvania 19122, United States
[‡]Department of Chemical Engineering, University of Pittsburgh, Pittsburgh, Pennsylvania 15261, United States
[§]Institute for Advanced Research and Department of Chemistry, Nagoya University, Nagoya 464-8602, Japan
[∥]Department of Applied Chemistry and Institute of Molecular Science, National Chiao Tung University, Hsinchu 30010, Taiwan

Supporting Information

ABSTRACT: Combined temperature-programmed desorption and IR studies suggest that absorption cross sections of IR-active vibrations of molecules "strongly" bound to single-wall carbon nanotubes (SWCNTs) are reduced at least by a factor of 10. Quantum chemical simulations show that IR intensities of endohedrally encapsulated molecules are dramatically reduced, and identify dielectric screening by highly polarizable SWCNT sidewalls as the origin of such "screening". The observed intensity reduction originates from a sizable cancellation of adsorbate dipole moments by mirror charges dynamically induced on the nanotube sidewalls. For exohedrally adsorbed molecules, the dielectric screening is found to be orientation-dependent with a smaller magnitude for adsorption in groove and interstitial sites. The presented results clearly demonstrate and quantify the screening effect of SWCNTs and unequivocally show that IR spectroscopy cannot be applied in a straightforward manner to the study of peapod systems.

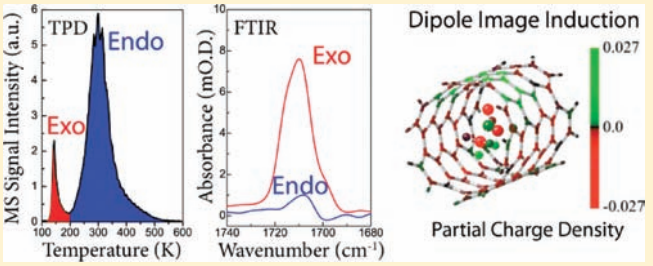

INTRODUCTION

Carbon nanotubes (CNTs) are ideally suited for the encapsulation of chemical species, with many possible applications.[1−7] It is therefore clear that effective experimental tools are required for the characterization of the encapsulated species. Transmission electron microscopy (TEM),[5,8−10] infrared (IR) spectroscopy,[9,11−13] Raman spectroscopy,[5,9,10,14,15] and nuclear magnetic resonance (NMR) spectroscopy[16,17] are experimental techniques widely used to characterize molecules encapsulated inside CNTs. In the case of vibrational spectroscopy, shifts in the position of IR- and Raman-active bands of encapsulated molecules or shifts in the vibrational spectroscopic features of CNTs are usually considered as evidence for encapsulation.[9−14,18] The corresponding changes in IR or Raman intensities received little attention, partly due to the difficulty of carrying out proper reference measurements.

However, IR, Raman, and NMR spectroscopic methods rely on the interaction of probe molecules with electromagnetic fields. Electronic structure calculations suggest that fullerenes and CNTs, due to the high polarizability of the delocalized π-electrons, can screen electric fields similar to a Faraday cage.[19−27] By the same token, CNT sidewalls are able to dielectrically screen electric charges in their vicinity.[28] For instance, it was shown theoretically that single-wall CNTs (SWCNTs) can screen dipoles of water chains by a factor of 4 independent of the tube or chain length,[22,29] and the dipole moment of a water molecule inside the fullerene C_{60} was predicted to be reduced roughly 3-fold.[20] Setyowati et al. explained the reduction of IR vibrational intensities of some vibrational modes of macromolecules adsorbed on the outside of CNT sidewalls[30] by the appearance of image dipoles in analogy with IR signal reduction of molecules adsorbed on metal surfaces.[31]

It is therefore rather surprising that *the magnitude of the IR intensity screening for molecules endohedrally adsorbed in CNTs has never been estimated*. In practice, we find that molecules "strongly" bound to CNTs are quasi-invisible to IR, and we theoretically investigated the cause of such "screening". Acetone, diethyl ether, and *n*-heptane were selected as probe molecules, since these molecules have distinct desorption energies on different sites of CNT bundles[32,33] and desorb molecularly from SWCNTs (see Figure S1 in the Supporting Information). The difference in desorption energies for molecules adsorbed on different adsorption sites of CNTs allows for the selective removal of species adsorbed less strongly (e.g., multilayers adsorbed outside the tubes, i.e., exohedrally) by flash-heating, leaving behind more strongly adsorbed molecules (e.g., in endohedral, groove, and interstitial sites) for spectroscopic investigation.

Received: October 2, 2010
Published: May 11, 2011

dx.doi.org/10.1021/ja108903u | *J. Am. Chem. Soc.* 2011, 133, 8191–8198

EXPERIMENTAL SECTION

Materials, Sample Preparation, and Pretreatment. SWCNTs produced by the high-pressure carbon monoxide (HiPco) method[34] (Carbon Nanotechnologies Inc., Houston TX) were air HCl purified in-house as described elsewhere.[33] Before introduction into the ultra-high-vacuum (UHV) chamber, SWCNTs were sonicated in acetone (Fisher, ACS grade) for 1 h and then deposited by the drop-and-dry method onto a W-grid (Alfa Aesar, 100 mesh, 0.002 in. wire diameter) in a flow of preheated air (~330 K). A fast response thermocouple (K-type, Omega) was spot-welded directly to the W-grid, which was then clamped to a metallic sample holder.[35] Analogous sample holders equipped with dewars were used in the temperature-programmed desorption (TPD) and IR experiments, allowing the temperature to be controlled from ~90 to 1400 K. Experiments were also performed on SWCNTs produced by the arc-discharge method (see the Supporting Information, section 1.3). After deposited sample was dried in a flow of hot air, its optical density was checked (~0.7−1.6 OD at 2000 cm^{-1}), the sample was placed inside the vacuum chamber and evacuated overnight to $<10^{-8}$ Torr. To clean the SWCNTs and decompose oxygen functionalities that might limit access to endohedral sites, SWCNTs were heated at 900 K for 30 min and then cooled to ~90−100 K under high vacuum.[33,36,37] After air/HCl purification SWCNTs have significant surface area exposed (Figure S9, Supporting Information), while vacuum annealing further opens access to the endohedral sites.[33,36,37] Before adsorbing probe molecules, the sample was flash-heated to 900 K and the temperature was quenched back to ~90−100 K.

TPD and IR Studies. The adsorbates were liquids (ACS reagent or HPLC grade). Before they were dosed in the vacuum chamber, the liquids were degassed by several (~4−7) freeze−pump−thaw cycles. The desired amount of adsorbate was dosed at $\sim 10^{-6}$ Torr through a leak valve to the sample cooled to 100 K. The background pressure before and after dosing was $\sim 5 \times 10^{-9}$ Torr. The heating rate was 2 K/s in all experiments. For TPD−MS experiments, samples were heated from 100 to 900 K with simultaneous collection of selected masses (AccuQuad RGA 300, Stanford Research Systems) corresponding to the most abundant fragments of the adsorbate. For control purposes, all masses in the 1−100 amu range were collected simultaneously in a number of experiments, and molecular desorption of adsorbates was verified in all cases (Figure S1 in the Supporting Information). The IR spectrum of the sample before adsorption of gases was used as a background in the IR experiments. After the desired amount of adsorbate was dosed to the sample, the spectrum was collected at 4 cm^{-1} resolution with an FTIR (Fourier Transform infrared) spectrometer (Tensor 27, Bruker). The flash-heating of gases in the IR experiments was done by heating the sample from ~100 K to the desired temperature (170 K for ethyl ether, 175 K for acetone, and 225 K for *n*-heptane). The objective of the flash-heating was the desorption of species having low desorption energy (adsorbed exohedrally and in multilayers).

COMPUTATIONAL METHODS

As in our previous studies,[33,38−40] we employed the damped London dispersion-augmented[41] self-consistent-charge density-functional tight-binding[42] (SCC-DFTB-D) method as the underlying quantum chemical potential for the theoretical calculations of acetone−SWCNT model systems. We employed DFTB parameters optimized for vibrational frequency calculations.[43−45] Equilibrium geometries were determined using stringent optimization criteria. All optimized geometries were characterized as minima on the potential energy surface by performing harmonic vibrational frequency analysis using analytical Hessians. The details of the IR spectral simulation are given in the Supporting Information, section 2.1. The employed methodology has been demonstrated[43,45−47] to give accuracy comparable to that of conventional DFT methods; test calculations reproduced reasonably accurate vibrational frequencies as well as IR intensities for pristine acetone[48,49] and SWCNTs[50,51] (Table S1 and Figures S10−S12,Supporting Information). Two types of semiconducting chiral SWCNTs with similar chiral angles have been used in our simulations: (6,5) (small diameter of 7.7 Å, model s) and (11,9) (large diameter of 14.0 Å, model l) SWCNTs. The models were open-ended and hydrogen-terminated and had a length of 10 Å. The HOMO−LUMO gaps were small but finite, with 1.18 eV for s and 0.50 eV for l. Groove sites and interstitial channels were modeled using two and three SWCNTs, respectively, aligned side by side. Possible combinations of s and l models result in three different groove sites (ss, ls, and ll) and four interstitial channels (sss, lss, lls, and lll). Analogous molecular models were employed in our previous studies of acetone−SWCNT interactions.[33,39] Atomic partial charges in isolated molecules (referred to as q) as well as in the molecule−SWCNT complexes (referred as to $\tilde{q}$) and the corresponding dipole moments were determined using Mulliken population analysis, which is the standard procedure in the SCC-DFTB framework. The difference between these two sets of charges is denoted as Δq and can be interpreted as charge fluctuation upon complex formation. Clearly, the charges and their fluctuations are dynamical quantities that vary during molecular vibrations. Here, we are particularly interested in the variation of atomic partial charges during the C═O bond stretch (referred to as δq). For details, see the Supporting Information, section 2.2. The charge fluctuations defined here will prove very useful to analyze the behavior of the IR intensities upon the complex formation. During the calculation of the vibrational frequencies and the corresponding eigenmodes, the hydrogen atoms terminating the SWCNT models were assigned masses of 10 000 amu to effectively remove their contributions from the spectra following the methodology applied in ref 47.

RESULTS AND DISCUSSION

IR and TPD Studies. Combined TPD and FTIR studies of acetone adsorbed on SWCNTs suggest that the cross sections of the ν(C═O) vibration (Figure 1) and other IR-active modes (Figure S5, Supporting Information) for "strongly" adsorbed acetone are significantly reduced in comparison with cross sections of more "weakly" adsorbed acetone. When 100 langmuirs of acetone is dosed to SWCNTs, the subsequent TPD spectra reveal two major peaks (Figure 1a). The peak at 300 K ("strong" physisorption) can be assigned to acetone desorption from endohedral sites, grooves, and accessible interstitial channels of SWCNTs.[33,39] The peak at 144 K ("weak" physisorption) can be assigned to desorption of acetone from SWCNT exohedral sites and multilayers.[33] The amount of "weakly" adsorbed acetone (red area under the 144 K peak) is ~10 times smaller than the amount of "strongly" adsorbed acetone (blue area under the peak at 300 K) (Figure 1a), suggesting that flash-heating to 200 K will eliminate "weakly" adsorbed acetone (~10% of total adsorbed acetone), leaving strongly adsorbed acetone (~90%). In addition, it is possible that the flash-heating also causes conversion of "weakly" bound species to "strongly" bound species that desorb with a peak at 300 K. We do not have direct evidence for this scenario; however, we discuss later its possible consequences.

Following the 100 langmuir dose of acetone on SWCNTs, the IR bands characteristic of physisorbed acetone were observed, with the most intense band at 1709 cm^{-1} assigned to the carbonyl bond (C═O) stretching mode (Figure 1b, black curve). On the basis of TPD results, one would expect a ~10% decrease in intensity of IR bands of acetone after removal of the "weakly" bound form by flash-heating to 200 K (Figure 1b, blue curve). However, an astounding ~90% decrease in intensity was

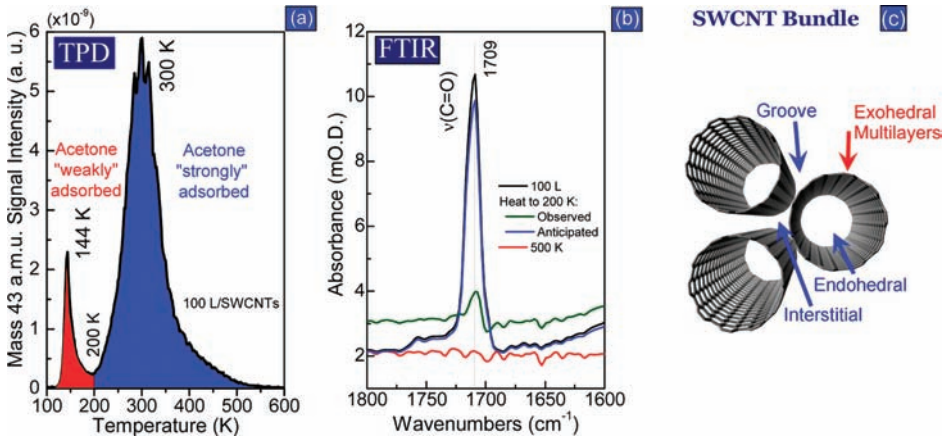

Figure 1. Screening of IR cross sections of the ν(C═O) mode of acetone adsorbed on HiPco SWCNTs. (a) According to TPD, the amount of acetone adsorbed on sites with low desorption energy (peak at 144 K) is ∼10% of the total amount of acetone desorbing after a 100 langmuir dose. Previously, the peak at 144 K was assigned to exohedral adsorption and adsorption in multilayers.[33] The rest (∼90%) is "strongly" bound acetone, peak at 300 K, previously assigned to endohedral adsorption.[33] (b) After adsorption of 100 langmuirs of acetone (black curve) and following flash-heating to 200 K, one would anticipate a ∼10% decrease in IR intensity (blue curve), while experimentally a ∼90% decrease in intensity was observed (green curve). (c) Schematic bundle of SWCNTs. The red arrow indicates sites with "weakly" adsorbed acetone (exohedral + multilayer adsorption), and blue arrows indicate sites with "strongly" adsorbed acetone (endohedral, groove, and accessible interstitial sites).[33,52]

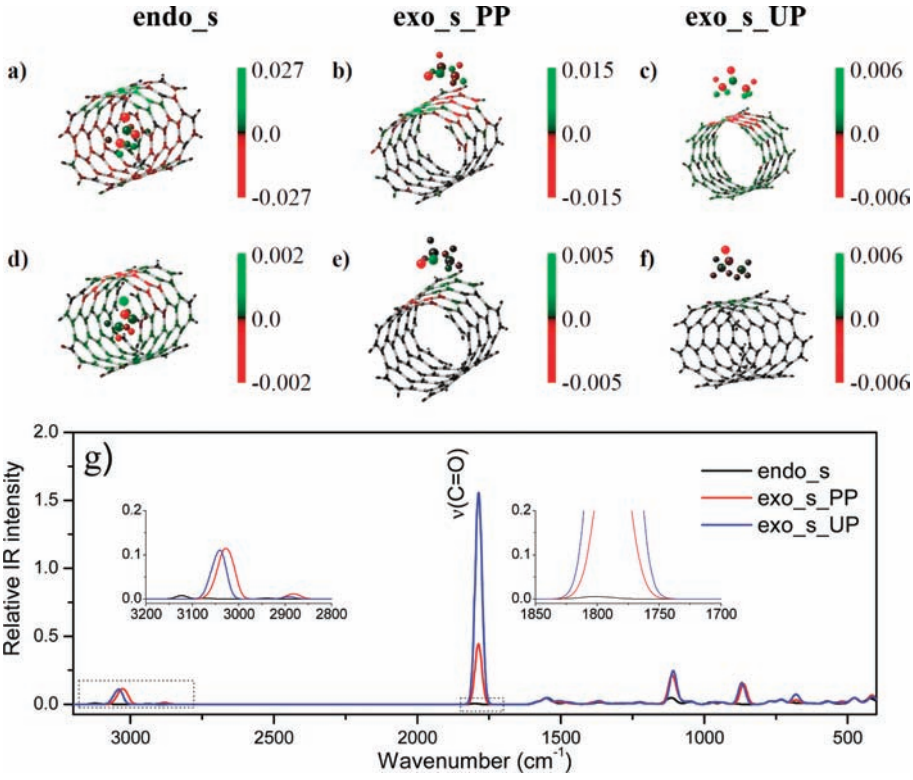

Figure 2. (a−c) Induced Mulliken charges Δq for acetone adsorbed endohedrally in a small nanotube (6,5) (endo_s), exohedrally on the (6,5) nanotube with the CCCO plane of acetone parallel to the SWCNT wall (exo_s_PP), and exohedrally with the C═O bond perpendicular to the SWCNT wall (exo_s_UP). (d−f) Dynamic charge fluctuations δq of the endo_s, exo_s_PP, and exo_s_UP complexes. (g) Theoretical vibrational IR spectra of endo_s, exo_s_PP, and exo_s_UP. IR intensities are given relative to the gas-phase acetone ν(C═O) band intensity scaled to unity. Corresponding plots for large-diameter tubes are given in the Supporting Information, section 2.4.

observed (Figure 1b, green curve). Consequently, the intensity of the ν(C═O) vibration of acetone adsorbed exohedrally or in multilayers is ∼10 times more intense than the ν(C═O) vibration of "strongly" adsorbed acetone (see Figure 1). A similar screening effect was observed for other acetone IR-active modes (Figure S5, Supporting Information). IR screening was also observed for acetone, ethyl ether, and *n*-heptane adsorbed on SWCNTs produced by arc-discharge (see the Supporting Information, section 1.3). It appears that all IR modes of "strongly" adsorbed molecules are screened to similar degrees. Given that

dx.doi.org/10.1021/ja108903u |*J. Am. Chem. Soc.* 2011, 133, 8191–8198

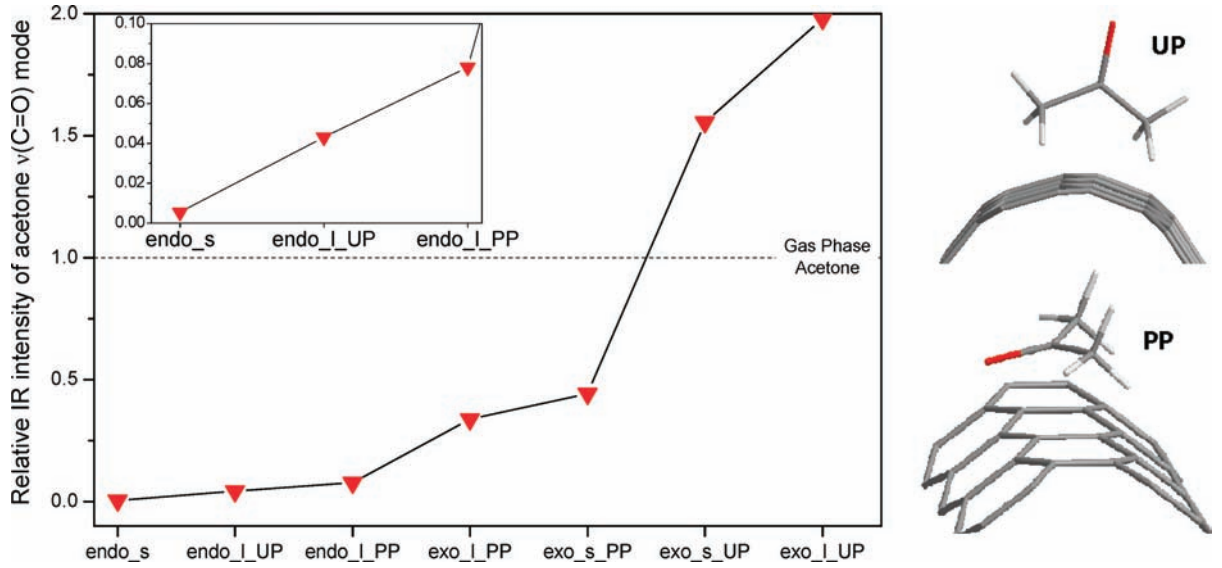

Figure 3. Theoretical IR intensities of the acetone ν(C═O) mode at around 1796 cm^{-1} for acetone−SWCNT complexes with different UP or PP equilibrium conformations (see the structures on the right) relative to the gas-phase acetone ν(C═O) band intensity.

not all adsorbate vibrational modes deform the molecule in the same direction relative to the carbon nanotube walls, this finding suggests that the orientation of the "strongly" bound adsorbates does not play a crucial role for the screening effectiveness.

Theoretical IR Spectra, Partial Atomic Charges, and Dipole Moments. Quantum chemical simulations confirm the experimentally observed dramatic IR screening for acetone adsorbed endohedrally inside single SWCNT model systems. In agreement with experiment, the computed IR intensities depend strongly on the adsorption site of acetone and its relative orientation to the tube wall. If acetone is absorbed endohedrally (endo), its IR activity is almost completely suppressed (see Figure 2g, black curve. A discussion of acetone dimensions relative to the available space inside small diameter tubes is given in the Supporting Information). In contrast, for acetone adsorbed exohedrally (exo), its vibrational bands become orders of magnitude more intense (see Figure 2g, red and blue curves) with magnitudes depending on the mutual alignment of the acetone molecular plane and the CNT sidewall. This behavior can be explained in terms of mirror charges (and consequently mirror dipole moments) induced by the adsorbed acetone on the nanotube walls.

To visualize the image charges induced on the SWCNT sidewalls, we analyzed two types of quantities: (i) charge redistribution Δq upon formation of the acetone−SWCNT complex and (ii) charge fluctuations δq during the C═O vibration. Figure 2 displays Δq, δq, and simulated IR spectra for acetone adsorbed on the s SWCNT model systems endohedrally (endo_s, left panel), exohedrally with PP conformation (exo_s_PP, middle panel), and exohedrally with UP conformation (exo_s_UP, right panel). Here, "PP" indicates a planar parallel orientation of the CCCO plane of acetone with respect to the CNT sidewall, and "UP" indicates an upward-pointing perpendicular orientation of the acetone C═O bond with respect to the nanotube sidewall (for further details, see Figure 3). First, we note that the induced charges Δq are approximately 10% of the partial atomic charges q. As can be inferred from Figure 2, the induced Mulliken charges Δq on the atoms of acetone are consistent with atomic electronegativities, while those on the carbon atoms of the SWCNT are simply the mirror charges induced by the vicinity of acetone atoms. Note

Table 1. Absolute Values of Dipole Moments (D) for the Acetone−SWCNT Complexes as Well as Their Acetone and SWCNT Components[a]

	μ(total)	μ(acetone)	μ(SWCNT)
acetone	2.330	2.330	
s	0.011		0.011
l	0.338		0.338
endo_s	0.140	2.469	2.589
endo_l_PP	0.612	2.405	1.996
endo_l_UP	0.877	2.317	1.444
exo_l_PP	1.359	2.303	1.322
exo_s_PP	1.518	2.329	0.865
exo_s_UP	3.057	2.461	0.609
exo_l_UP	3.120	2.504	0.633

[a] Note the quite different orientations of the dipole components in some complexes. s, small-diameter SWCNT (6,5); l, large-diameter SWCNT (11,9); UP and PP, perpendicular and parallel orientations of C═O mode to SWCNT wall, respectively; endo and exo, endohedral and exohedral adsorption of acetone, respectively.

that an infinitely long, isolated nanotube is electrostatically neutral. However, the large number of mirror point charges on the SWCNT and relatively large distances between the centers of the positive and negative charge are still capable of producing sizable dipole moments. The energy required for the charge redistribution is almost negligible, owing to the large polarizability of the nanotube and the small magnitude of the induced charges. We point out that the model systems selected are not formally metallic, indicating that metallicity is not a required property for CNTs to display nearly perfect dielectric screening.

We find that the degree of IR intensity screening follows the order endohedral ≫ exohedral adsorption with acetone in the PP conformation, while complexes with acetone adsorbed exohedrally in the UP conformation experience an enhancement of the IR intensity (Figure 2). This closely resembles the situation encountered in IR spectroscopy of adsorbates on metal surfaces.[31,53,54]

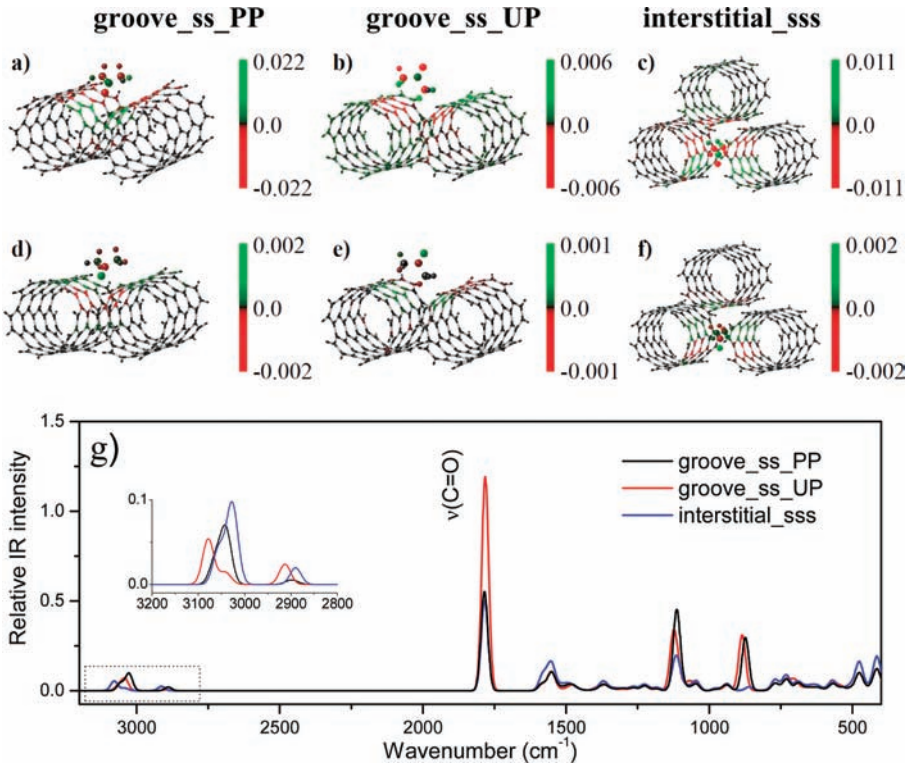

Figure 4. Induced Mulliken charges Δq (a−c) and dynamic charge fluctuations δq (d−f) of acetone adsorbed (from left to right) on a groove site constructed using two small nanotubes (6,5) with the C═O axis parallel to the trough (groove_ss_PP), on a groove site constructed using two small nanotubes (6,5) with the C═O axis perpendicular to the trough (groove_ss_UP), and in interstitial sites constructed using three small nanotubes (6,5) (interstitial_sss). (g) Theoretical vibrational IR spectra of the groove_ss_PP, groove_ss_UP, and interstitial_sss models with IR intensities given relative to the gas-phase acetone ν(C═O) band intensity scaled to unity.

The magnitude of intensity reduction strongly varies, as shown in Figure 3. The intensity ratio between the gas-phase IR intensity (=1.0) and that in endo_s (∼0.005) is ∼180, while the analogous ratio in the case of acetone adsorbed on large (11, 9) nanotubes (exo_l_UP) is only ∼0.5. It is found that, in the case of exohedral complexes, the total dipole moment (see Table 1) and the intensity (Figure 3) are reduced when the C═O bond is parallel (PP) to the wall and that the total dipole moment and the intensity are constructively enhanced when the C═O bond is perpendicular (UP) to the wall. The larger diameter l CNT model is more efficient in screening of endo- and exohedrally adsorbed acetone with the PP conformation (screening occurs parallel to the sidewall) than the small-diameter s CNT model.

The dielectric screening reduces the total dipole moment from 2.33 D in the gas phase to 1.52 D (∼1.5-fold reduction) for the exo_s_PP form and to 0.14 D (∼17-fold reduction) for the endo_s configuration (Table 1). The actual magnitude of the acetone dipole moment in the complexes varies only slightly from the gas-phase value (Table 1). Almost all the shielding effect originates from the induced dipole moment on the nanotube. According to the theoretical results, the shielding for endohedral adsorption is not perfect (Figure 2), possibly due to the finite length of the SWCNT models used in the calculations. Nevertheless, those results explain the intensity patterns in the IR spectra (Figure 1).

Analogous theoretical simulations were performed for complexes where acetone is adsorbed in groove sites or interstitial channels. For groove site adsorption, we categorized the possible complex structures into two classes: (i) PP with the C═O bond parallel to the plane defined by the two tube axes and (ii) UP with the C═O bond pointing upward and perpendicular to the plane defined by the two tube axes. For the interstitial site adsorption, we considered only one structure with acetone located in the plane perpendicular to the tube axes and the C═O bond pointing away from the channel center, which appears to be energetically favorable in comparison with other possible conformations. Figure 4 depicts induced Mulliken charges Δq, dynamic charge fluctuations δq, and the calculated IR spectra for model systems composed of an acetone molecule adsorbed on a bundle of aligned s SWCNTs. The corresponding results obtained with l and mixed s/l SWCNT models are presented in the Supporting Information. The analysis of the induced charges for acetone adsorbed inside grooves and interstitial sites shows that the magnitudes of Δq and δq are of the same order as in the case of a single-tube *exohedral* site adsorption, but the mirror charges are spread among all participating nanotube components. Therefore, it is not surprising that the IR spectra shown in Figure 4 are similar to those discussed earlier for the single-tube *exohedral* complexes. Figure 5 summarizes simulated IR intensities of the acetone ν(C═O) mode. For groove sites, it is found that the degree of the ν(C═O) IR signal reduction/enhancement and its dependence on the orientation of the C═O bond display characteristics very similar to those discussed above for single-tube exohedral adsorption sites. For the interstitial sites, the IR signal always experiences a reduction with a magnitude comparable to that of the groove PP complexes, which can be explained by the competition of the IR enhancement and reduction effects due to simultaneously occurring relative UP and PP acetone−SWCNT conformations.

dx.doi.org/10.1021/ja108903u |*J. Am. Chem. Soc.* 2011, 133, 8191–8198

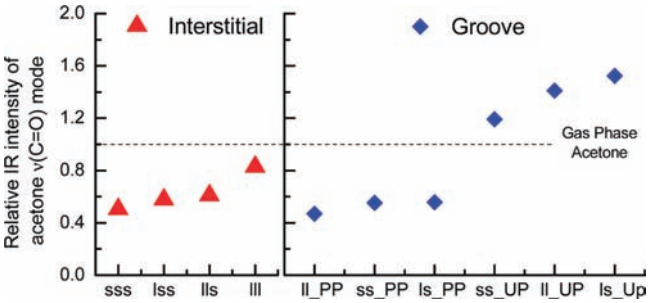

Figure 5. Theoretical IR intensities of the acetone ν(C═O) mode at around 1796 cm^{-1} for acetone−SWCNT bundle complexes at optimized geometries relative to the gas-phase acetone ν(C═O) band intensity.

Table 2. Absolute Values of Dipole Moments (D) for the Acetone−SWCNT Bundle Complexes as Well as Acetone and SWCNT Components of the Complexes

	μ(total)	μ(acetone)	μ(SWCNTs)
acetone	2.330	2.330	
ss	0.537		0.537
ls	0.382		0.382
ll	0.705		0.705
sss	0.545		0.545
lss	0.537		0.537
lls	0.970		0.970
lll	1.697		1.697
groove_ss_PP	1.692	2.338	1.199
groove_ss_UP	2.791	2.434	0.485
groove_ls_PP	1.635	2.351	1.292
groove_ls_UP	2.721	2.467	0.565
groove_ll_PP	2.143	2.300	1.846
groove_ll_UP	2.284	2.433	0.583
interstitial_sss	1.788	2.614	0.879
interstitial_lss	2.204	2.622	0.570
interstitial_lls	2.640	2.544	0.771
interstitial_lll	1.666	2.559	1.841

Table 2 lists the calculated dipole moments for the acetone−SWCNT bundle complexes as well as their individual components. In close analogy with the single-tube adsorption (see Table 1), the dipole moment magnitudes for the acetone component located in various environments remain practically constant. Again, almost all the shielding effect originates from the image dipole moment induced on the SWCNT sidewall by the adsorbate.

Implications of IR Reduced Cross Sections of Molecules Adsorbed on SWCNTs. We have shown experimentally that molecules (acetone, diethyl ether, *n*-heptane) adsorbed presumably endohedrally, in grooves, and in accessible interstitial channels of SWCNTs, produced by different techniques (arc-discharge and HiPco), have reduced effective IR cross sections in comparison with molecules adsorbed exohedrally and in multilayers. The theoretical simulations of acetone−SWCNT complexes confirm the experimentally observed dramatic reduction of IR vibrational cross sections for molecules encapsulated in carbon nanotubes and, to a lesser degree, of molecules adsorbed in interstitial channels and exohedrally in grooves when their transition dipole moments are aligned parallel to the walls of the SWCNTs. The results of theoretical consideration of endohedrally adsorbed acetone suggest that the intensity of the ν(C═O) mode should be reduced at least 10-fold (Figure 3), well in agreement with experiment (Figure 1a). We believe that the desorption peak observed at 300 K (Figure 1a) was composed mainly of endohedrally adsorbed acetone with a possible admixture of acetone at groove sites and accessible interstitial channels.[33] The fraction of acetone molecules adsorbed in groove sites and accessible interstitial channels might be responsible for the weak peak observed in the IR spectrum after flash-heating (Figure 1b). For acetone located in groove sites, with parallel dipole orientation, and interstitial channels, the simulated IR intensity reduction is relatively small, reaching maximally 50% (Figure 5). Clearly, if a large portion of the "strongly" adsorbed acetone molecules were located in these sites, the experimentally observed IR signal in Figure 1b would be significantly larger. This conjecture is supported by the fact that for adsorption in groove sites and interstitial channels, the simulations (Figure 4) predict quite different degrees of screening for various vibrational modes of acetone, which is in contrast with the experiment, where all the modes seem to be uniformly screened (Figure S5, Supporting Information). Hence, adsorption in mainly endohedral sites is consistent with experiment as the simulated screening is quite uniform for all vibrational modes of encapsulated acetone.

As mentioned above, the low-temperature adsorption may lead to a nonequilibrium distribution of adsorbates; e.g., easily accessible exohedral sites (low desorption energy) might be already saturated, while endohedral sites (desorption energy) are still not filled completely. Flash-heating to 200 K (Figure 1) can lead only to partial desorption of exohedrally adsorbed species, while some of the molecules can migrate to endohedral sites. However, in this case the estimated screening effect would be even stronger.

Although the effect reported here does not come as a surprise given the large number of studies on Faraday shielding[21−27] and static dipole screening[20,22,29] in the literature, the dramatic magnitude of the IR cross section reduction for molecules adsorbed in CNTs and their bundles has never been reported before and is quantified here for the first time. The effect of screening was not explicitly considered in previous publications.[9,11−13]

SUMMARY

The presented experimental data suggest that molecules "strongly" bound to SWCNTs have effective cross sections of IR-active modes that are reduced at least by a factor of 10 in comparison with molecules adsorbed exohedrally (Figure 1). This screening effect occurs with different choices of adsorbed molecules and nanotubes (Supporting Information, section 1.3). Quantum chemical simulations of IR spectra confirm the more than 10-fold reduction of IR cross sections for endohedrally adsorbed molecules (Figure 3) and up to 2-fold reduction for molecules adsorbed in interstitial channels. Species adsorbed exohedrally or in groove sites may experience only partial screening or constructive transition dipole moment enhancement, depending on the relative orientation of their transition dipole moments to the tube sidewall (Figures 3 and 5). IR intensity reduction for groove and interstitial sites is comparable in magnitude to adsorption on single-tube exohedral sites. According to the simulated IR spectra, the metallicity (size of the HOMO−LUMO gap) of the SWCNT models does not play a

role in the observed screening effect. Our findings have important implications for the spectroscopy of CNTs. The dramatic reductions of IR cross sections can amount effectively to the observed screening effect, making the molecules adsorbed inside CNTs practically invisible to IR and possibly to other experimental techniques utilizing electromagnetic radiation.

■ ASSOCIATED CONTENT

Supporting Information. Additional information to support the experimental and theoretical findings. This material is available free of charge via the Internet at http://pubs.acs.org.

■ AUTHOR INFORMATION

Corresponding Author

eborguet@temple.edu; sirle@iar.nagoya-u.ac.jp; hwitek@mail.nctu.edu.tw

Author Contributions

⊥These authors contributed equally.

■ ACKNOWLEDGMENT

S.I. acknowledges support by the Program for Improvement of Research Environment for Young Researchers from the Ministry of Education, Culture, Sports, Science and Technology (MEXT) of Japan, by a Japan Science and Technology Agency/Core Research for Evolutional Science and Technology grant in the area of "High Performance Computing for Multiscale and Multiphysics Phenomena", and by a Grant-in-Aid (KAKENHI) from the Japan Society for the Promotion of Science in Priority Area "Molecular Theory for Real Systems". H.A.W. acknowledges financial support from the National Science Council of Taiwan (Grants NSC96-2113-M-009-022 and NSC99-2113-M-009-011) and the ATU project of the Ministry of Education, Taiwan. E.B. and D.V.K. acknowledge the support of the Department of Energy, Office of Basic Energy Sciences. We acknowledge the help of Dr. Nikolay Dementev in conducting the volumetric adsorption measurements.

■ REFERENCES

(1) Smith, B. W.; Monthioux, M.; Luzzi, D. E. *Nature* **1998**, *396*, 323.
(2) Leonhardt, A.; Ritschel, M.; Kozhuharova, R.; Graff, A.; Muhl, T.; Huhle, R.; Monch, I.; Elefant, D.; Schneider, C. M. *Diamond Relat. Mater.* **2003**, *12*, 790.
(3) Bianco, A.; Kostarelos, K.; Partidos, C. D.; Prato, M. *Chem. Commun.* **2005**, 571.
(4) Noy, A.; Park, H. G.; Fornasiero, F.; Holt, J. K.; Grigoropoulos, C. P.; Bakajin, O. *Nano Today* **2007**, *2*, 22.
(5) Pan, X.; Fan, Z.; Chen, W.; Ding, Y.; Luo, H.; Bao, X. *Nat. Mater.* **2007**, *6*, 507.
(6) Santiso, E. E.; George, A. M.; Turner, C. H.; Kostov, M. K.; Gubbins, K. E.; Buongiorno-Nardelli, M.; Sliwinska-Bartkowiak, M. *Appl. Surf. Sci.* **2005**, *252*, 766.
(7) Shiozawa, H.; Pichler, T.; Grüneis, A.; Pfeiffer, R.; Kuzmany, H.; Liu, Z.; Suenaga, K.; Kataura, H. *Adv. Mater.* **2008**, *20*, 1443.
(8) Smith, B. W.; Monthioux, M.; Luzzi, D. E. *Chem. Phys. Lett.* **1999**, *315*, 31.
(9) Wang, J.; Marina, K. K.; Poliakoff, M.; Briggs, G. A. D.; Khlobystov, A. N. *Angew. Chem., Int. Ed.* **2006**, *45*, 5188.
(10) Li, Y. F.; Hatakeyama, R.; Kaneko, T.; Izumida, T.; Okada, T.; Kato, T. *Nanotechnology* **2006**, *17*, 4143.
(11) Matranga, C.; Chen, L.; Smith, M.; Bittner, E.; Johnson, J. K.; Bockrath, B. *J. Phys. Chem. B* **2003**, *107*, 12930.
(12) Byl, O.; Kondratyuk, P.; Forth, S. T.; FitzGerald, S. A.; Chen, L.; Johnson, J. K.; Yates, J. T., Jr. *J. Am. Chem. Soc.* **2003**, *125*, 5889.
(13) Byl, O.; Liu, J. C.; Wang, Y.; Yim, W. L.; Johnson, J. K.; Yates, J. T. *J. Am. Chem. Soc.* **2006**, *128*, 12090.
(14) Nishide, D.; Dohi, H.; Wakabayashi, T.; Nishibori, E.; Aoyagi, S.; Ishida, M.; Kikuchi, S.; Kitaura, R.; Sugai, T.; Sakata, M.; Shinohara, H. *Chem. Phys. Lett.* **2006**, *428*, 356.
(15) Wenseleers, W.; Cambre, S.; Culin, J.; Bouwen, A.; Goovaerts, E. *Adv. Mater.* **2007**, *19*, 2274.
(16) Sekhaneh, W.; Kotecha, M.; Dettlaff-Weglikowska, U.; Veeman, W. S. *Chem. Phys. Lett.* **2006**, *428*, 143.
(17) Chen, Q.; Herberg, J. L.; Mogilevsky, G.; Wang, H. J.; Stadermann, M.; Holt, J. K.; Wu, Y. *Nano Lett.* **2008**, *8*, 1902.
(18) Witek, H. A.; Trzaskowski, B.; Małolepsza, E.; Morokuma, K.; Adamowicz, L. *Chem. Phys. Lett.* **2007**, *446*, 87.
(19) Delaney, P.; Greer, J. C. *Appl. Phys. Lett.* **2004**, *84*, 431.
(20) Yagi, K.; Watanabe, D. *Int. J. Quantum Chem.* **2009**, *109*, 2080.
(21) Lou, L.; Nordlander, P.; Smalley, R. E. *Phys. Rev. B: Condens. Matter Mater. Phys.* **1995**, *52*, 1429.
(22) Lu, D.; Li, Y.; Rotkin, S. V.; Ravaioli, U.; Schulten, K. *Nano Lett.* **2004**, *4*, 2383.
(23) Chen, S. C.; Hseih, W. C.; Lin, M. F. *Phys. Rev. B: Condens. Matter Mater. Phys.* **2005**, *72*, 193412/1.
(24) Sebastiani, D.; Kudin, K. N. *ACS Nano* **2008**, *2*, 661.
(25) Brothers, E. N.; Scuseria, G. E.; Kudin, K. N. *J. Chem. Phys.* **2006**, *124*, 041101/1.
(26) Brothers, E. N.; Izmaylov, A. F.; Scuseria, G. E.; Kudin, K. N. *J. Phys. Chem. C* **2008**, *112*, 1396.
(27) Uchida, K.; Oshiyama, A. *Phys. Rev. B* **2009**, *79*, 235444/1.
(28) Lin, M. F.; Chuu, D. S. *Physical Review B: Condens. Matter Mater. Phys.* **1997**, *56*, 4496.
(29) Mann, D. J.; Halls, M. D. *Phys. Rev. Lett.* **2003**, *90*, 195503/1.
(30) Setyowati, K.; Piao, M. J.; Chen, J.; Liu, H. *Appl. Phys. Lett.* **2008**, *92*, 043105.
(31) Pearce, H. A.; Sheppard, N. *Surf. Sci.* **1976**, *59*, 205.
(32) Kondratyuk, P.; Yates, J. T., Jr. *Acc. Chem. Res.* **2007**, *40*, 995.
(33) Kazachkin, D.; Nishimura, Y.; Irle, S.; Morokuma, K.; Vidic, R. D.; Borguet, E. *Langmuir* **2008**, *24*, 7848.
(34) Nikolaev, P.; Bronikowski, M. J.; Bradley, R. K.; Rohmund, F.; Colbert, D. T.; Smith, K. A.; Smalley, R. E. *Chem. Phys. Lett.* **1999**, *313*, 91.
(35) Kwon, S.; Borguet, E.; Vidic, R. D. *Environ. Sci. Technol.* **2002**, *36*, 4162.
(36) Kuznetsova, A.; Mawhinney, D. B.; Naumenko, V.; Yates, J. T.; Liu, J.; Smalley, R. E. *Chem. Phys. Lett.* **2000**, *321*, 292.
(37) Kuznetsova, A.; Popova, I.; Yates, J. T., Jr.; Bronikowski, M. J.; Huffman, C. B.; Liu, J.; Smalley, R. E.; Hwu, H. H.; Chen, J. G. *J. Am. Chem. Soc.* **2001**, *123*, 10699.
(38) Feng, X.; Irle, S.; Witek, H. A.; Morokuma, K.; Vidic, R.; Borguet, E. *J. Am. Chem. Soc.* **2005**, *127*, 10533.
(39) Kazachkin, D.; Nishimura, Y.; Irle, S.; Feng, X.; Vidic, R.; Borguet, E. *Carbon* **2010**, *48*, 1867.
(40) Witek, H. A.; Irle, S.; Zheng, G.; de Jong, W. A.; Morokuma, K. *J. Chem. Phys.* **2006**, *125*, 214706/1.
(41) Elstner, M.; Hobza, P.; Frauenheim, T.; Suhai, S.; Kaxiras, E. *J. Chem. Phys.* **2001**, *114*, 5149.
(42) Elstner, M.; Porezag, D.; Jungnickel, G.; Elsner, J.; Haugk, M.; Frauenheim, T.; Suhai, S.; Seifert, G. *Phys. Rev. B: Condens. Matter Mater. Phys.* **1998**, *58*, 7260.
(43) Małolepsza, E.; Witek, H. A.; Morokuma, K. *Chem. Phys. Lett.* **2005**, *412*, 237.
(44) Witek, H. A.; Irle, S.; Morokuma, K. *J. Chem. Phys.* **2004**, *121*, 5163.
(45) Witek, H. A.; Morokuma, K.; Stradomska, A. *J. Theor. Comput. Chem.* **2005**, *4*, 639.

(46) Witek, H. A.; Morokuma, K. *J. Comput. Chem.* **2004**, *25*, 1858.
(47) Li, W.; Irle, S.; Witek, H. A. *ACS Nano* **2010**, *4*, 4475.
(48) Rogers, J. D.; Rub, B.; Goldman, S.; Person, W. B. *J. Phys. Chem.* **1981**, *85*, 3725.
(49) Max, J.-J.; Chapados, C. *Chem. Phys. Lett.* **2004**, *120*, 6627.
(50) Jeon, G. S.; Mahan, G. D. *Physical Review B: Condens. Matter Mater. Phys.* **2005**, *72*, 155415/1.
(51) Chen, S. C.; Shyu, F. L.; Lue, C. S.; Lin, M. F. *Physica E (Amsterdam)* **2006**, *32*, 577.
(52) Kwon, S.; Russell, J.; Zhao, X.; Vidic, R. D.; Johnson, J. K.; Borguet, E. *Langmuir* **2002**, *18*, 2595.
(53) Borguet, E.; Dai, H. L. *J. Phys. Chem. B* **2005**, *109*, 8509.
(54) Borguet, E.; Dai, H. L. *Chem. Phys. Lett.* **1992**, *194*, 57.